To cite this article: ZHANG S S, LIU J, ZHANG P, et al. Response of carbon fiber trapezoidal corrugated sandwich structure under air explosion loading [J/OL]. Chinese Journal of Ship Research, 2023, 18(2). http://www.ship-research.com/en/article/doi/10.19693/j.issn.1673-3185.02573.

DOI: 10.19693/j.issn.1673-3185. 02573

Response of carbon fiber trapezoidal corrugated sandwich structure under air explosion loading

ZHANG Shuaishuai, LIU Jun, ZHANG Pan, CHENG Yuansheng*

School of Naval Architecture and Ocean Engineering, Huazhong University of Science and Technology, Wuhan 430074, China

Abstract: [**Objectives**] The effects of the thickness of the face sheet, angle of the wall plate and height of the core layer on the anti-explosion performance of carbon fiber reinforced composite trapezoidal corrugated sandwich structures were investigated. [**Methods**] First, based on the 3D Hashin failure criterion, a subroutine module of the damage evolution of fiber reinforced composites is developed using the VUMAT user subroutine interface in ABAQUS. Second, through comparison with experiments in the public literature, the effectiveness of the dynamic response simulation method of carbon fiber reinforced composites based on a development subroutine under explosion impact loading is verified. Finally, a parametric study on the explosion resistance of carbon fiber reinforced composite trapezoidal corrugated plates is carried out based on the numerical method. [**Results**] The results show that, compared with increasing the thickness of the blast face sheet, increasing the thickness of the back blast face sheet can improve the explosion resistance of the sandwich plate more obviously; when the folding angle of the core wall plate decreases from 45° to 30°, the explosion resistance increases by 1.3%; when it decreases from 60° to 45°, the explosion resistance increases by 6.3%; and when the core height increases from 8 mm to 20 mm, the explosion resistance increases by 27.7%. [**Conclusions**] The results of this study can provide references for the explosion-proof design of carbon fiber reinforced composite sandwich structures.

Key words: composite; blast impact; trapezoidal corrugated plate; damage evolution; ABAQUS

CIC number: U661.5; U668.5

0 Introduction

Compared with traditional metal materials, carbon fiber reinforced polymer (CFRP) offers the advantages of small specific gravity, high strength, and high designability. It is thus widely used in military fields, such as ships, aircraft, and tanks, and its anti-explosion performance has received increasingly more attention.

Yazid et al. [1] found in an experimental approach that various damages, such as fiber buckling on the front surface, fiber fracture on the back surface, and shear failure at the clamping boundary, could be observed on plain-weave CFRP laminates of different thicknesses under blast impact, while interlayer delamination mainly occurred in the mid-thickness area of the laminates. Langdon et al [2-4] studied many factors affecting the mechanical properties of fiber reinforced composites, including structural form, laminate thickness, and lamination angle. The damage modes of fiber reinforced composites under blast impact mainly include interlayer delamination,

Received: 2021 − 10 − 26 **Accepted**: 2022 − 03 − 23

Authors: ZHANG Shuaishuai, male, born in 1996, master 's degree candidate. Research interest: explosion impact dynamics. E-mail: 1944736757@qq.com

LIU Jun, male, born in 1981, Ph.D., associate professor. Research interests: structural analysis and lightweight design and structural vibration and impact resistance analysis. E-mail: hustlj@hust.edu.cn

ZHANG Pan, male, born in 1986, Ph.D., associate professor. Research interests: structural optimization design and explosion and impact resistance. E-mail: panzhang@hust.edu.cn

CHENG Yuansheng, male, born in 1962, Ph.D., professor, doctoral supervisor. Research interest: marine ship structure optimization design. E-mail: yscheng@hust.edu.cn

***Corresponding author**: LIU Jun

fiber fracture, debonding at the fiber and matrix interface, and matrix cracking, and they usually coexist. Plain-weave composites provide better anti-explosion performance than that of composites characterized by unidirectional lamination. Xin et al. [5-6] proposed a progressive damage model based on the fracture energy method to predict the response and failure of laminates made from fiber reinforced composites under impact loading. Zhao et al. [7] studied the energy dissipation mechanism of foam sandwich plates by combining numerical simulation with experiment. The results showed that the energy dissipation effect of sandwich plates was better than that of solid plates under the same conditions and that the energy dissipation effect was the best in the case of a thin front face sheet and a thick back face sheet. Li et al. [8] used numerical simulation software to study the anti-explosion performance of functionally graded aluminum foam sandwich plates. The results revealed that the density arrangement of the sandwich plate core had a great influence on the energy dissipation effect of the sandwich plate.

The current research on the anti-explosion performance of CFRPs mainly has the following problems:

1) The dynamic response process of the structure is difficult to obtain in the blast impact experiment. Moreover, the blast impact involves complex processes, such as shock wave propagation and fluid-solid interaction, which add to the difficulty in analyzing the failure mechanism of the structure.

2) CFRP is brittle to a certain extent, compared with metal materials featuring good ductility. Consequently, the internal damage is difficult to evaluate with the naked eye when CFRP is subjected to blast impact loading.

3) Accurately predicting the damage evolution of composites is difficult as the damage evolution criteria for them in the current commercial finite element software are mostly two-dimensional.

On the above basis, the authors of this paper will focus on the CFRP trapezoidal corrugated plate and study its anti-explosion performance by numerical simulation. Specifically, the user-defined subroutine interface VUMAT in software ABAQUS is used to write a subroutine based on the 3D-Hashin[9] failure criterion and thereby simulate the damage evolution of fiber reinforced composites. Then, the experimental results in public literature are used for verification. Finally, the authors calculate and analyze the effects of the thicknesses of the upper and lower face sheets, the folding angle of the wall plate, and the core height on the anti-explosion performance of CFRP trapezoidal corrugated sandwich structures. This paper is expected to provide references for the explosion-proof design of CFRP sandwich structures.

1 Calculation model

1.1 Finite element model

The trapezoidal corrugated sandwich structure comprised an upper plate, a lower plate, and a core in the middle, which were all made from CFRP in this study. The carbon fiber (T300-3K) was a plain-weave structure, and the matrix was the vinyl resin (430LV).

The length and width of the trapezoidal corrugated plate were 280 mm × 280 mm. Square fixtures of the same size were placed on both sides of the corrugated plate, and rigid body constraints were applied to the fixtures to simulate the clamping effect on the target plate. Circular openings with a radius of 100 mm were created in the center of the fixtures to serve as the load-bearing surface for the blast impact and the deformation area in the target plate. Only a 1/4 scaled model was constructed, and the corresponding symmetrical boundary conditions were applied to the model in the numerical calculation, due to the symmetry of the sandwich plate and the blast loading. The woven structure outperforms one characterized by unidirectional lamination in integrity, with the same material properties in the transverse and longitudinal directions of the lamination. The directions of the fiber and the matrix in traditional unidirectional lamination were denoted by Direction 1 and Direction 2, respectively, to avoid ambiguity. Fig. 1(a) presents the definitions of the two directions and the related dimensions of the trapezoidal corrugated structure.

The in-plane grid size of the structure was about 1 mm, and the number of grids in the direction of thickness was the same as that of laminated layers, with each layer being 0.26 mm thick. To simulate delamination failure, the authors adopted the cohesive element (COH3D8) with a cohesive thickness of 0.01 mm (Fig. 1(b)).

The coupled Eulerian-Lagrangian (CEL) method in the software ABAQUS was used to simulate the

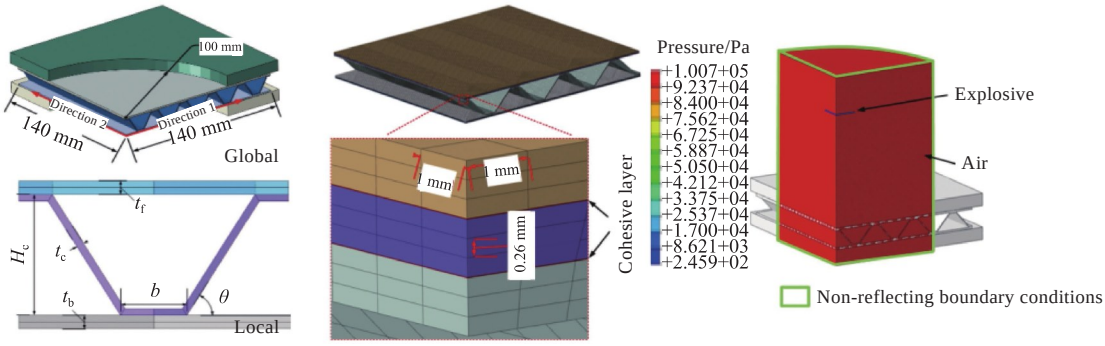

(a) Geometry of structure (b) Grid division of structure (c) Euler domain

Fig. 1 Numerical model of CFRP trapezoidal corrugated plate under blast loading

blast impact loading. Specifically, Euler grids filled with multiple materials were defined, and the non-reflecting boundary conditions were applied to the outer surface of the Euler domain to simulate the infinite air domain. The Euler grids were kept at the size of 1 mm and filled with the PE4 explosive to prevent the shock wave pressure to attenuate excessively fast, and the remaining area was filled with air, as shown in Fig. 1(c). The charge of the PE4 explosive was 2 g and the stand-off distance was 90 mm in all the conditions calculated in this study.

The thickness t_f of the front face panel, the thickness t_b of the back face panel, the folding angle θ of the core wall plate, and the core height H_c were taken as variables according to the structural characteristics of the trapezoidal corrugated plate to study the influence of each variable on the anti-explosion performance of the trapezoidal corrugated sandwich plate. The thickness of the core was 0.78 mm, and the width of the platform was 7 mm, as shown in Fig. 1(a).

1.2 Material model

1.2.1 Composite

The Hashin failure criterion has been widely used in numerical simulation of the explosion and impact of composite materials [3, 10 - 11]. The built-in material model in ABAQUS only complies with the 2D-Hashin failure criterion and does not take into account the damage mode of interlayer delamination. For this reason, the authors adopted the subroutine interface in ABAQUS to write the strain-based 3D-Hashin failure criterion in the FORTRAN language and thereby predict the properties of composites more accurately.

The Hashin failure criterion divides the damage to composite materials into four modes, namely, fiber tension, fiber compression, matrix tension, and matrix compression, but these damage modes are specific to unidirectional lamination. In contrast, the authors defined the damage to plain-weave carbon fiber into tension and compression in Direction 1 and Direction 2, respectively. To characterize the damage among the laminated layers of composites, the authors introduced the interlayer damage mode by referring to the Ye [12] criterion.

A total of five damage factors were introduced into the calculation model, namely, the tensile damage factor e_{ft} in Direction 1, the compressive damage factor e_{fc} in Direction 1, the tensile damage factor e_{mt} in Direction 2, the compressive damage factor e_{mc} in Direction 2, and the interlayer damage factor e_{ld}. They can be calculated by Eqs. (1) – (5), respectively. Material damage occurs when the damage factor $e_i > 0$ (i = ft, fc, mt, mc, ld).

$$e_{ft}^2 = \left(\frac{\varepsilon_{11}}{X_t^\varepsilon}\right)^2 - 1 \begin{cases} \geqslant 0 & \text{failed} \\ < 0 & \text{elastic} \end{cases} \tag{1}$$

$$e_{fc}^2 = \left(\frac{\varepsilon_{11}}{X_c^\varepsilon}\right)^2 - 1 \begin{cases} \geqslant 0 & \text{failed} \\ < 0 & \text{elastic} \end{cases} \tag{2}$$

$$e_{mt}^2 = \left(\frac{\varepsilon_{22}}{Y_t^\varepsilon}\right)^2 - 1 \begin{cases} \geqslant 0 & \text{failed} \\ < 0 & \text{elastic} \end{cases} \tag{3}$$

$$e_{mc}^2 = \left(\frac{\varepsilon_{22}}{Y_c^\varepsilon}\right)^2 - 1 \begin{cases} \geqslant 0 & \text{failed} \\ < 0 & \text{elastic} \end{cases} \tag{4}$$

$$e_{ld}^2 = \left(\frac{\varepsilon_{33}}{Z_t^\varepsilon}\right)^2 + \left(\frac{\varepsilon_{13}}{S_{13}^\varepsilon}\right)^2 + \left(\frac{\varepsilon_{12}}{S_{12}^\varepsilon}\right)^2 - 1 \begin{cases} \geqslant 0 & \text{failed} \\ < 0 & \text{elastic} \end{cases} \tag{5}$$

where ε is the strain; X_t^ε, Y_t^ε, X_c^ε, and Y_c^ε are the strains corresponding to the tensile strength and compressive strength in Direction 1 and Direction 2, respectively; Z_t^ε is the strain corresponding to the tensile strength in the direction perpendicular to the lamination; S_{13}^ε and S_{12}^ε are the strains under the shear strength perpendicular to the lamination; the subscripts 11 and 22 denote the positive sides of Direction 1 and Direction 2, respectively; the subscript 33 indicates the direction of thickness; the

subscripts 12 and 13 represent the plane perpendicular to Directions 1 and 2 and the one perpendicular to Direction 1 and 3, respectively. The material parameters of plain-weave CFRP laminates are listed in Table 1.

Table 1 Parameters of plain-weave CFRP laminates [13]

Paramter	Value
Elastic modulus E_{11} in Direction 1/GPa	62.3
Elastic modulus E_{22} in Direction 2/GPa	62.3
Elastic modulus E_{33} in direction of thickness/GPa	8.5
Poisson's ratios ν_{12}, ν_{13}, and ν_{23}	0.06
Shear modulus G_{12}/GPa	7.1
Shear moduli G_{13} and G_{23}/GPa	3
Tensile strength X_t in Direction 1/MPa	610
Compressive strength X_c in Direction 1/MPa	314.7
Tensile strength Y_t in Direction 2/MPa	610
Compressive strength Y_c in Direction 2/MPa	314.7
Tensile strength Z_t in direction of thickness/MPa	55.6
Compressive strength Z_c in direction of thickness/MPa	500
Shear strength S_{12}/MPa	101.7
Shear strength S_{13} and S_{23}/MPa	59.4
Density ρ/(kg·m^{-3})	1 467

The damage variable H_i ($0 \leqslant H_i \leqslant 1$) was introduced to characterize the damage degree of the material. H_i=0 is the starting point of material damage; H_i=1 indicates that the material fails completely and the element is deleted; the stiffness matrix of the material degenerates when $0 < H_i < 1$, and a larger H_i corresponds to a more substantial reduction of the stiffness matrix. The above design suggests that the damage variable H_i can be fitted by the following equation:

$$H_i = \begin{cases} 0, & e_i < 0 \\ \dfrac{1}{e_i^n}, & e_i \geqslant 0 \end{cases} \tag{6}$$

where n is a dimensionless constant and can control the evolution speed of the damage variable H_i. The authors set n = 0.55 after trial calculation as it is closer to the experimental results.

1.2.2 Cohesive element

The cohesive element (COH3D8) is a unique element in ABAQUS to simulate the cohesive effect, and two categories are defined in simulation and calculation, namely, damage initiation and damage evolution.

Damage initiation is determined by the following equation:

$$\left(\frac{\sigma_n}{\sigma_N}\right)^2 + \left(\frac{\sigma_s}{\sigma_S}\right)^2 + \left(\frac{\sigma_t}{\sigma_T}\right)^2 = 1 \tag{7}$$

where σ_N, σ_S, and σ_T are the maximum tensile stress in the direction normal to the cohesive plane and the maximum shear stresses on the two orthogonal planes, respectively; σ_n, σ_s, and σ_t are the tensile stress in the direction normal to the cohesive plane and the shear stresses on the two orthogonal planes in the actual calculation. A judgment is made that the damage to the cohesive element starts and the element enters the stage of damage evolution when the sum of the squares of the three items in Eq. (7) is equal to one. The evolution process is controlled by energy, and the cohesive element is deleted when the following equation holds

$$\left(\frac{G_n}{G_N}\right) + \left(\frac{G_s}{G_S}\right) + \left(\frac{G_t}{G_T}\right) = 1 \tag{8}$$

In Eq. (8), G_N, G_S, and G_T are the tensile fracture energy in the direction normal to the cohesive plane and the shear fracture energy on the two orthogonal planes, respectively; G_n, G_s, and G_t are the corresponding dissipated energy in the actual calculation. The material parameters of the cohesive element are listed in Table 2.

Table 2 Material parameters of cohesive element [3]

Paramter		Value
Elastic moduli	E_{11}/GPa	4.3
	G_{12}/GPa	2.0
	G_{13}/GPa	2.0
Failure stresses	σ_N/MPa	100
	σ_S/MPa	80
	σ_T/MPa	80
Fracture energy	G_N/(J·m^{-2})	1 500
	G_S/(J·m^{-2})	2 000
	G_T/(J·m^{-2})	2 000

1.2.3 Explosive and air

The Euler domain was filled with explosives and air, with the PE4 explosive described by the Jones-Wilkins-Lee (JWL) state equation and air described by the ideal gas state equation. The specific parameters are presented in Tables 3−4.

2 Effectiveness verification of numerical method

2.1 Numerical model

To verify the effectiveness of the proposed numerical model, the authors selected the results of

Table 3 Parameters in JWL state equation for PE4 explosive [13]

Paramter	Value
Density/(kg·m^{-3})	1 770
A/GPa	617.5
B/GPa	16.9
R_1	4.4
R_2	1.2
ω	0.25
Detonation velocity V/(m·s^{-1})	7 100
Initial internal energy E_m/(J·kg^{-1})	5.707×10^6

Note: A, B, R_1, R_2, and ω are the parameters in the JWL state equation.

Table 4 Parameters in gas state equation for air [14]

Paramter	Value
Density/(kg·m^{-3})	1.225
Atmospheric pressure/Pa	1.013×10^5
Volume constant R	287.05
Initial temperatre θ/℃	20
Absolute zero θ_z/℃	–273

the blast impact experiment on plain-weave CFRP in Ref. [1] for comparative verification. Similarly, the modeling method of constructing a 1/4 scaled model was adopted, and the corresponding symmetrical boundary conditions were applied to the symmetrical surface. In the experiments, the equivalent of the PE4 explosive was 2 g, and the detonation distance was 90 mm. The experimental specimen was a square laminated plate made from plain-weave CFRP. A steel fixture was placed on both sides of the specimen, and rigid body constraints were applied to it to simulate the clamping effect on the specimen (Fig. 2(a)). The steel pipe where the explosive was placed would reflect the shock wave. For this reason, a circular steel pipe was also created in the numerical model to satisfy the rigid body constraints. The contact between the medium in the Euler domain and the inner surface of the steel pipe was set to implement the reflection effect of the steel pipe on the shock wave, as shown in Fig. 2(a). The side length of the laminate was 150 mm, and the circular surface in the middle with a diameter of 90 mm was the blast impact area. The grid size in the circular loading area on the specimen was 1 mm, and that in the clamping area was 2 mm. The number of laminated layers was eight, and each layer was 0.26 mm thick, as shown in Fig. 2(b) and Fig. 2(c).

2.2 Calculation results

Circular shear failure occurred on the clamping boundary of the plain-weave CFRP laminate under blast impact loading, and cross-shaped cracks appeared in the center of the laminate. The crack lengths were 34 and 34.5 mm, respectively (Fig. 3(a)). The laminate fractured on the front face at its clamping boundary when the specimen was cut along the center line after the experiment. Moreover, clear delamination could be observed in the mid-thickness area of the laminate, with a delamination length of 12.1 mm (Fig. 3(b)).

In the numerical simulation results, the state variable S_{DV} represents the tensile damage and compressive damage in Direction 1 and Direction 2. According to Fig. 3(c), the damage to the laminate is mainly concentrated at its clamping boundary and in its center, and the maximum value of the damage variables is invariably above 0.95. This indicates that the material in the red area is almost completely damaged and that the element is about to be deleted. The superimposition of the four damage variables suggests that the damage at the clamping boundary is roughly circular while that in the central area is cross-shaped. The crack length is 34 mm when S_{DV}=0.8 is taken as the crack boundary, as shown in Fig. 3(a). The damage profile in Fig. 3(b) reveals that serious damage occurs at the clamping boundary and that evident delamination damage also occurs in the mid-thickness area on the

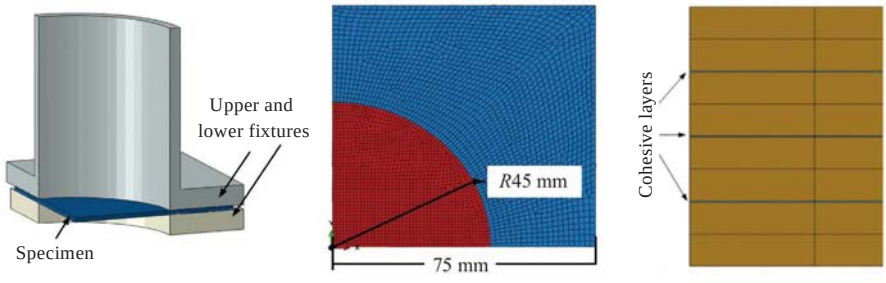

(a) Overall geometric model (b) Grid division (c) Cohesive element

Fig. 2 Numerical model of CFRP laminate

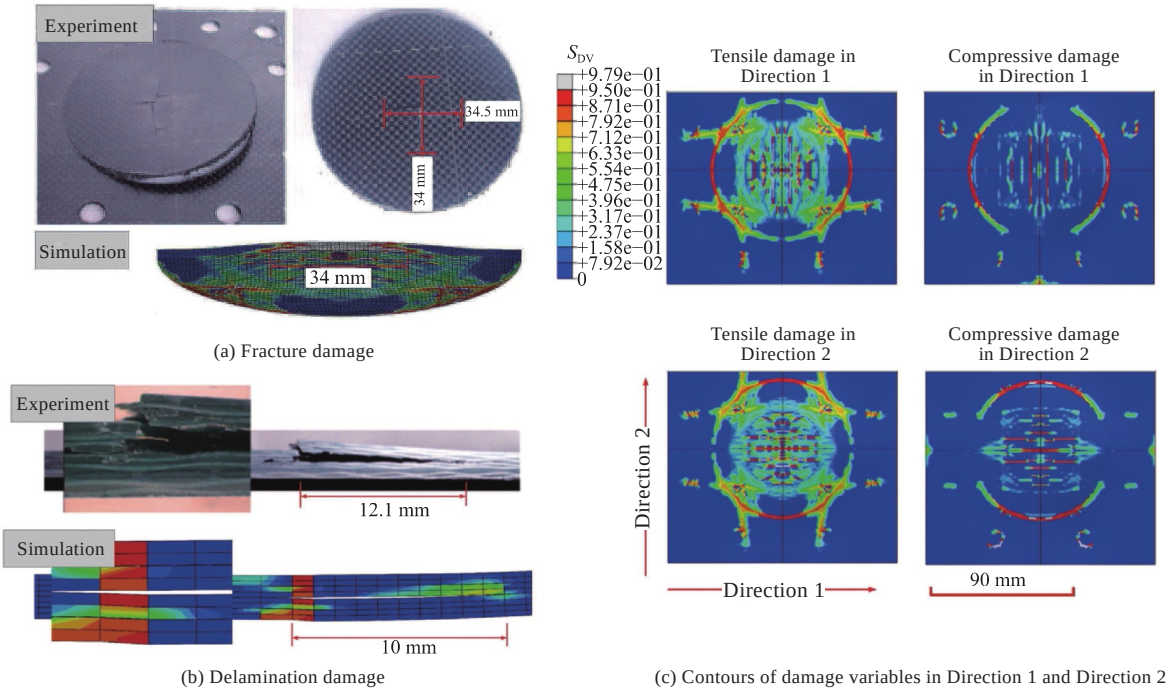

(a) Fracture damage

(b) Delamination damage

(c) Contours of damage variables in Direction 1 and Direction 2

Fig. 3 Comparison of experimental and simulation results [1]

laminate, with a delamination length of 10 mm.

The above results reveal that the CFRP laminate in the experiment presents salient damage characteristics that are generally consistent with those in the numerical calculation results. The error in the length of the cross-shaped cracks is within 2%, and that in the length of the delamination damage is about 17.5%, indicating that the numerical simulation method is reasonable and effective.

3 Calculation results and analysis

A total of four sets of calculation conditions were designed to investigate the influences of the thicknesses of the upper and lower face sheets (0.78, 1.56, and 2.34 mm), the folding angle of the core wall plate (30°, 45°, and 60°), and the core height (8, 14, and 20 mm) on the sandwich structure (Table 5).

Table 5 Parameter design of trapezoidal corrugated sandwich plate

Condition	Thickness t_f of front face sheet/mm	Thickness t_b of back face sheet/mm	Core height H_c/mm	Folding angle θ of core wall plate/(°)	Relative mass per unit area
TC-1	1.56	1.56	14	45	1.00
TC-2	0.78	1.56	14	45	0.81
TC-3	2.34	1.56	14	45	1.19
TC-4	1.56	0.78	14	45	0.81
TC-5	1.56	2.34	14	45	1.19
TC-6	1.56	1.56	14	30	0.97
TC-7	1.56	1.56	14	60	1.05
TC-8	1.56	1.56	8	45	0.99
TC-9	1.56	1.56	20	45	1.01

3.1 Dynamic response process of structure

The typical dynamic response process of the trapezoidal corrugated sandwich plates under blast impact loading was described by taking the TC-1 condition as an example. The pressure in the air-filled area was about one standard atmospheric pressure at the initial moment. The detonation products and the shock wave spread rapidly to the surrounding area with the explosive-filled area as the center after the explosive was detonated. In this case, the pressure inside and at the boundary of the shock wave exceeded 20 MPa, as shown in Fig. 4(a) and Fig. 4(b). The front face sheet of the sandwich structure began to deform under compression when the shock wave reached it. However, the deformation of the front face sheet was non-uniform since the platform area on the trapezoidal corrugated core provided strong support for the upper plate, as shown in Fig. 4(c) and Fig. 4(d). The non-uniform deformation of the front face sheet caused delamination damage in its mid-thickness area, as shown in Fig. 4(e). The upper plate supported by the platform also showed substantial deformation as the transfer of the blast impact loading continued, which led to the serious buckling deformation of the core (Figs. 4(e)−4(f)). The deformation of the back face sheet gradually increased as the blast

impact loading further transferred from the core to the back face sheet. In contrast, the front face sheet entered the rebound stage at this time. The lagging deformation of the back face sheet turned the core in compression into one in tension, consequently resulting in more serious delamination between the front face sheet and the core (Fig. 4(g)). The deformation ranges of the plates on both sides and the core expanded due to the transmission of the stress wave and the connection within the structure. Nevertheless, the deformation became uniform, as shown in Fig. 4(h).

As shown in Fig. 5, the maximum deformation at the center of the front face sheet is 8.62 mm and occurs at about 0.1 ms under the blast impact loading, and that at the center of the back face sheet is 5.23 mm. The maximum velocity at the center of the front face sheet is much larger than that of the back face sheet as the former can reach 200 m/s while the latter is not more than 100 m/s. The velocity trend of the back face sheet obviously lags behind that of the front face sheet in the time histories of velocity.

Fig. 6 presents the contours of the damage variables of the structure. It shows that the trapezoidal corrugated sandwich plate is mainly subject to tensile damage in Direction 1, with the most severe damage at the core. This is because the core buckles markedly under blast impact loading, resulting in a large tensile strain in Direction 1. The damage to the front face sheet is mainly concentrated on the upper surface of its joint with the core platform. The reason is that the deformation in this area is not uniform under the restriction of the core platform, resulting in a large tensile strain in Direction 1. The damage to the back face sheet is mainly manifested as compressive damage in Direction 1. This can be attributed to the compression of the back face sheet by the core during the transfer of the impact loading, as shown in Figs. 6(a) − (d). The delamination damage can mainly be divided into four types, namely, the delamination of the front face sheet, the delamination of the back face sheet,

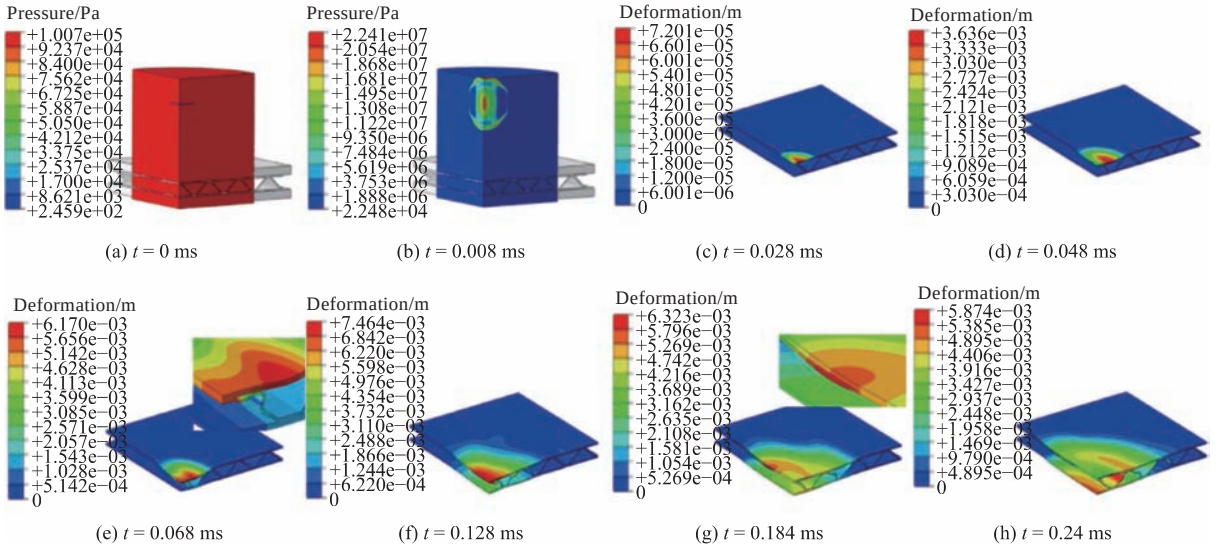

(a) t = 0 ms (b) t = 0.008 ms (c) t = 0.028 ms (d) t = 0.048 ms

(e) t = 0.068 ms (f) t = 0.128 ms (g) t = 0.184 ms (h) t = 0.24 ms

Fig. 4 Dynamic response process of trapezoidal corrugated plate under blast impact loading

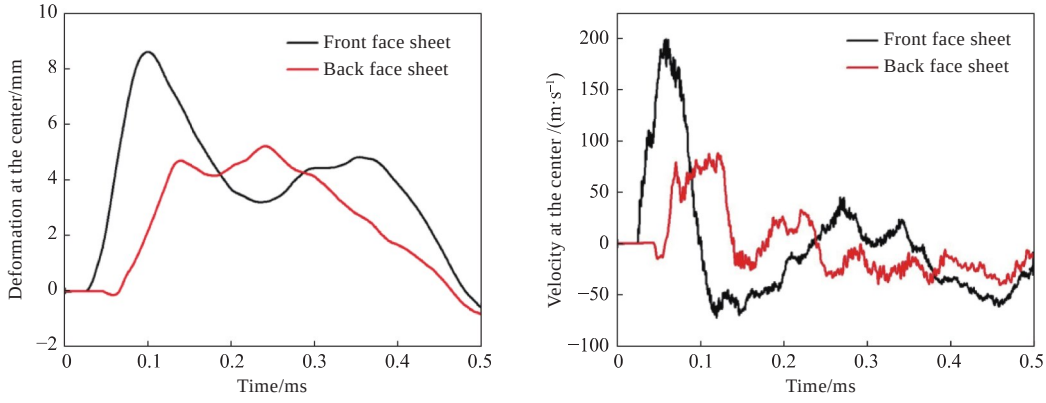

(a) Time histories of deformations of face sheets on both sides (b) Time histories of veoicies of face sheets on boh sides

Fig. 5 Time histories of deformation and velocity of face sheets on both sides

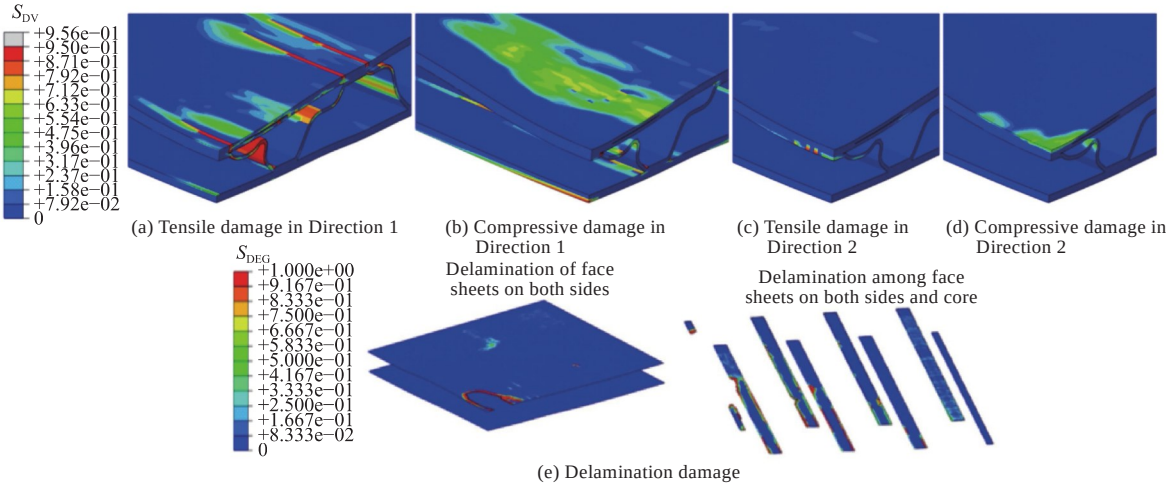

Fig. 6 Damage to trapezoidal corrugated plate made from fiber reinforced composite

that between the front face sheet and the core, and that between the back face sheet and the core. Among them, the delamination damage to the front face sheet is mainly concentrated in the central blast impact area, and the delamination damage in Direction 2 is more severe than that in Direction 1; the back face sheet undergoes no delamination. The damage to the cohesive element among the plates on both sides and the core is mainly manifested as follows: The delamination damage between the front face sheet and the core is greater than that between the back face sheet and the core; the delamination damage in direction 2 is greater than that in Direction 1; the delamination damage is mostly concentrated at the edge of the platform area on the core (Fig. 6(e)). In the figure, S_{DEG} is the damage state variable of the cohesive layer.

3.2 Influence of face sheet thickness on dynamic response of structure

In this aspect, the authors investigated the responses of trapezoidal corrugated sandwich plates with front face sheets of three different thicknesses and back face sheets of three different thicknesses, respectively, under the same blast impact loading.

The center of the front face sheet is most affected by blast impact loading. A thinner front face sheet corresponds to more serious damage, more evident delamination, and even complete material damage. In the last case, surface damage occurs, and the subsequent blast impact loading directly acts on the core, consequently aggravating the buckling deformation of the core. The impact resistance of the front face sheet and the overall stiffness of the structure enhance as the thickness of the front face sheet increases. Moreover, the deformations at the center of the front face sheet and the back face sheet decrease, with a salient decrease in the deformation of the front face sheet (Fig. 7(a)). The tensile damage in Direction 1 is taken as an example for analysis. The results reveal that the tensile damage to the front face sheet decreases as the thickness of the front face sheet increases. In addition, the buckling deformation of the core decreases due to the enhanced overall stiffness of the structure, leading to a decrease in tensile damage (Fig. 7(b)). In the figure, S_{DV1} is the damage state variable in Direction 1.

The overall stiffness of the structure improves as the thickness of the back face sheet increases, and the overall deformation of the structure decreases. The delamination damage increases slightly as the deformation at the center of the front face sheet decreases slightly. The reason is that thickening the back face sheet will also increase the inertia force of the back face sheet, and the back face sheet imposes a stronger counterforce on the front face sheet in this case, which reduces the deformation at the center of the front face sheet. Nevertheless, the stronger counterforce aggravates the uneven deformation of the front face sheet, resulting in more serious delamination damage. A thicker back face sheet means higher stiffness and strength. As a result, the deformation at the center of the back face sheet will decrease significantly as the back face sheet thickens (Fig. 8(a)). Similarly, the tensile damage in Direction 1 was analyzed as an example. The results reveal that as the thickness of the back face sheet increases, the damage to the front face sheet does not change markedly. In contrast, the tensile damage to the core caused by buckling deformation becomes more serious, and the damage to the back face sheet decreases significantly, as shown in Fig. 8(b).

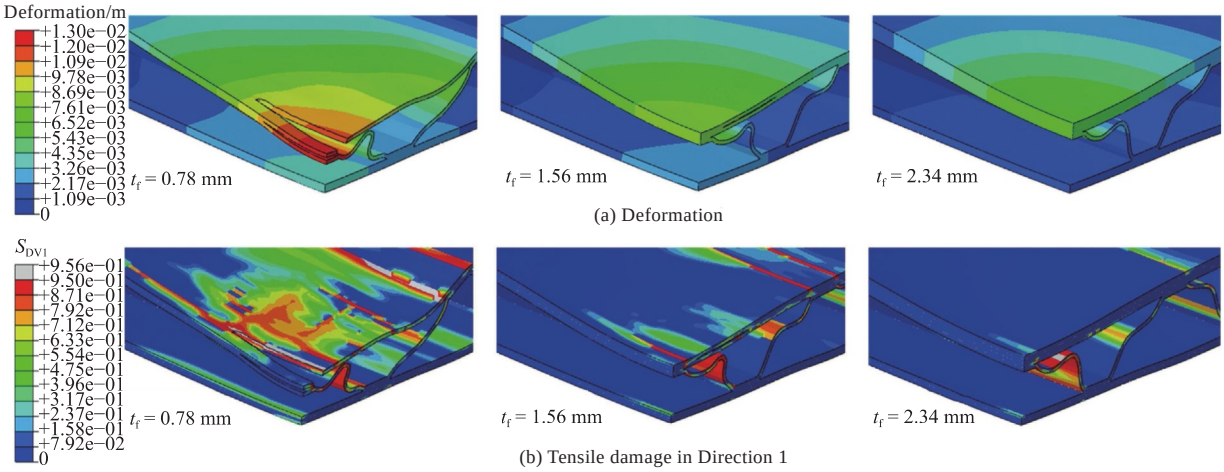

Fig. 7 Responses of trapezoidal corrugated plates with front face sheets of different thicknesses

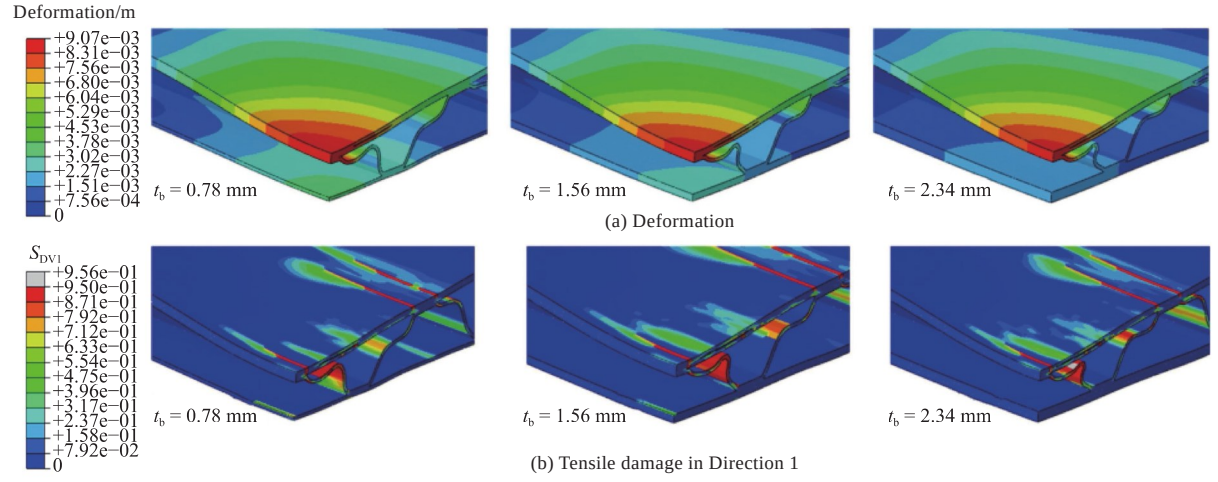

Fig. 8 Response of trapezoidal corrugated plates with back face sheets of different thicknesses

The explosion resistance of the trapezoidal corrugated sandwich plate can be enhanced by thickening either the front face sheet or the back face sheet if the maximum deformation at the center of the back face sheet is taken as the evaluation criterion for the anti-explosion performance of the sandwich plate. Figs 9(a) −9(b) show that the explosion resistance of the sandwich plate increases by 5.1% when the thickness of the front face sheet increases from 1.56 mm to 2.34 mm. The increase is 10% when the thickness of the back face sheet rises from 1.56 mm to 2.34 mm. In summary, thickening the back face sheet is more effective than thickening the front one, as shown in Fig. 9(c).

3.3 Influence of folding angle of core wall plate on dynamic response of structure

In this aspect, the authors examined the responses of trapezoidal corrugated sandwich plates

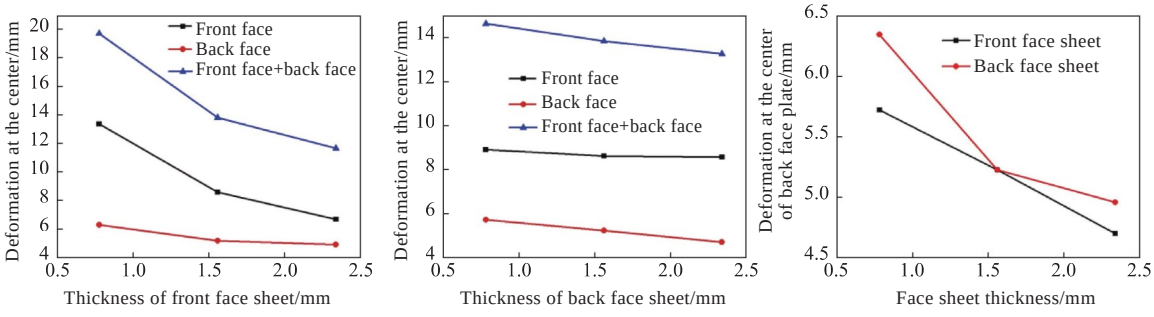

(a) Under an invariable thickness of 1.56 mm of back face sheet and different thicknesses of front face sheet

(b) Under an invariable thickness of 1.56 mm of front face sheet and different thicknesses of back face sheet

(c) Under different thicknesses of face sheets on both sides

Fig. 9 Maximum deformation curves of trapezoidal corrugated plates with different face sheet thicknesses

with core wall plates of three different folding angles under the same blast impact loading. The analysis of the calculation results indicates that the support the core provides for the front face sheet enhances as the folding angle of the core wall plate increases, and the overall stiffness of the structure rises accordingly, ultimately reducing the deformation of both the front face sheet and the overall structure; the uneven deformation of the front face sheet worsens, resulting in more serious delamination damage to the front face sheet; the enhancement of the support the core provides also results in the transfer of more impact loading from the core to the back face sheet. Consequently, the delamination damage between the core and the back face sheet aggravates, and the deformation at the center of the back face sheet increases accordingly (Fig. 10(a)). The contours of the tensile damage in Direction 1 suggest that the damage to the front face sheet does not change markedly as the folding angle of the core wall plate rises, while that of the back face sheet increases saliently. Moreover, the damage to the core is most serious when the folding angle θ of the wall plate is 45°, and the damage range of the core is the largest when θ is 60°. The reason is that a larger folding angle of the core wall plate corresponds to a smaller span of the trapezoidal corrugated core. When θ is 60°, two core wall plates undergo buckling deformation, and their tensile damage is smaller than that in the case of only one core wall plate subject to instability, as shown in Fig. 10(b).

Table 5 shows that the change in the weight of the structure caused by that in the folding angle of the wall plate is insignificant and thus largely negligible. The explosion resistance of the trapezoidal corrugated sandwich plate increases by 6.3% when the folding angle of the core wall plate is reduced from 60° to 45° if the maximum deformation at the center of the back face sheet is taken as the evaluation criterion for the anti-explosion performance of the sandwich plate. The increase is only 1.3% when the folding angle is reduced from 45° to 30°, as shown in Fig. 10(c). Therefore, the anti-explosion performance of the sandwich plate can be improved by reducing the folding angle of the core wall plate within a particular range. Nevertheless, the effect is trivial when the folding angle is reduced from 45° to 30°.

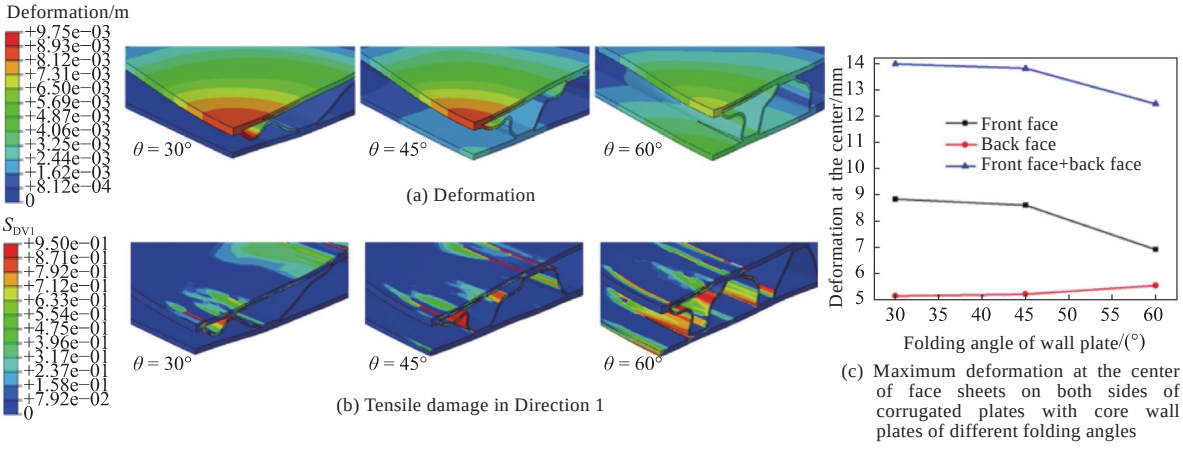

Fig. 10 Responses of trapezoidal corrugated plates with different folding angles

3.4 Influence of core height on dynamic response of structure

The authors also explored the responses of trapezoidal corrugated sandwich plates with three different core heights under the same blast impact loading. The analysis of the calculation results reveals that the overall stiffness of the structure increases as the core height rises, and the overall deformation of the structure decreases accordingly; a higher core will lead to a larger span of the wall plates. Consequently, the core is more likely to become unstable under the action of the blast impact, ultimately weakening the support it provides. Then, the deformation at the center of the front face sheet will increase, but the delamination damage to the front face sheet will decrease. Moreover, the deformation at the center of the back face sheet will decrease accordingly, as shown in Fig. 11(a). The contours of the tensile damage in Direction 1 shown in Fig. 11(b) suggest that the damage to the face sheets on both sides does not change significantly while the damage to the core decreases as the core height increases.

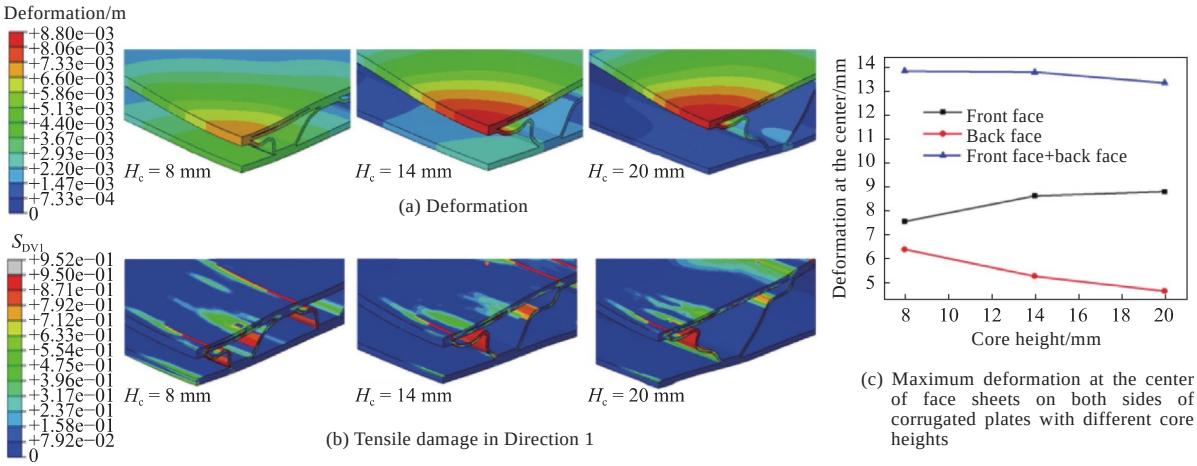

Fig. 11 Responses of trapezoidal corrugated plates with different core heights

According to Table 5, the change in the weight of the structure caused by that in the core height is also insignificant and thus essentially negligible. The maximum deformation at the center of the back face sheet is taken as the evaluation criterion for the anti-explosion performance of the trapezoidal corrugated sandwich plate. In this case, the explosion resistance of the sandwich plate increases by 27.7% when the core height is raised from 8 mm to 20 mm, as shown in Fig. 11(c). Therefore, the anti-explosion performance of the sandwich plate can be improved by increasing the core height. Nevertheless, increasing the core height will not only lead to a larger weight of the structure but also result in more space resources occupied in practical applications, which requires designers to make a trade-off according to the actual situation.

4 Conclusions

The authors constructed a numerical model of the progressive damage and failure of composites in compliance with the 3D-Hashin failure criterion and compared the results with the experimental counterparts. Then, they investigated the parametrization of carbon fiber all-composite trapezoidal corrugated sandwich plates oriented towards anti-explosion performance with the model constructed. The main conclusions are as follows:

1) The numerical simulation results can be used to effectively predict CFRP's damage characteristics and response process under blast impact loading.

2) The explosion resistance of the sandwich plate increases by 5.1% when the thickness of the front face sheet rises from 1.56 mm to 2.34 mm. The increase is 10% when the thickness of the back face sheet rises from 1.56 mm to 2.34 mm. Therefore, the anti-explosion performance of the trapezoidal corrugated sandwich plate can be improved by increasing either the thickness of the front face sheet or that of the back face sheet. In addition, increasing the thickness of the back face sheet can improve the anti-explosion performance of the sandwich plate more substantially than thickening the front face sheet.

3) The explosion resistance of the sandwich plate can be increased by 6.3% when the folding angle of the core wall plate is reduced from 60° to 45°. In contrast, the increase is only 1.3% when the folding angle is reduced from 45° to 30°. In summary, anti-explosion performance can be enhanced by reducing the folding angle of the core wall plate within a particular range. Nevertheless, the improvement in the anti-explosion performance is trivial when the reduction is from 45° to 30°.

4) The explosion resistance of the sandwich plate is improved by 27.7% when the core height is increased from 8 mm to 20 mm. The anti-explosion performance of the trapezoidal corrugated sandwich plate can be enhanced by increasing the core height to the extent allowed by the space configuration and weight control.

References

[1] YAZID YAHYA M, CANTWELL W J, LANGDON G S, et al. The blast resistance of a woven carbon fiber-reinforced epoxy composite [J]. Journal of Composite Materials, 2011, 45(7): 789−801.

[2] LANGDON G S, CANTWELL W J, GUAN Z W, et al. The response of polymeric composite structures to airblast loading: a state-of-the-art [J]. International Materials Reviews, 2014, 59(3): 159−177.

[3] LANGDON G S, KARAGIOZOVA D, von KLEMPERER C J, et al. The air-blast response of sandwich panels with composite face sheets and polymer foam

cores: experiments and predictions [J]. International Journal of Impact Engineering, 2013, 54: 64−82.

[4] LANGDON G S, von KLEMPERER C J, ROWLAND B K, et al. The response of sandwich structures with composite face sheets and polymer foam cores to air-blast loading: preliminary experiments [J]. Engineering Structures, 2012, 36: 104−112.

[5] XIN S H, WEN H M. A progressive damage model for fiber reinforced plastic composites subjected to impact loading [J]. International Journal of Impact Engineering,2015, 75: 40−52.

[6] XIN S H, WEN H M. Numerical study on the perforation of fiber reinforced plastic laminates struck by high velocity projectiles [J]. The Journal of Strain Analysis for Engineering Design, 2012, 47(7): 513−523.

[7] ZHAO Y J, HAO Y, LIU J H, et al. Energy dissipation mechanism of foam sandwich plate subjected to contact underwater explosion [J]. Chinese Journal of Ship Research, 2018, 13(3): 13−22 (in Chinese).

[8] LI C P, ZHANG P, LIU J, et al. Numerical simulation of dynamic response of functionally graded aluminum foam sandwich panels under air blast loading [J]. Chinese Journal of Ship Research, 2018, 13(3): 77−84 (in Chinese).

[9] HASHIN Z. Failure criteria for unidirectional fiber composites [J]. Journal of Applied Mechanics, 1980, 47(2): 329−334.

[10] GARGANO A, DAS R, MOURITZ A P. Finite element modelling of the explosive blast response of carbon fibre-polymer laminates [J]. Composites Part B: Engineering, 2019, 177: 107412.

[11] MOURITZ A P. Advances in understanding the response of fibre-based polymer composites to shock waves and explosive blasts [J]. Composites Part A: Applied Science and Manufacturing, 2019, 125: 105502.

[12] YE L. Role of matrix resin in delamination onset and growth in composite laminates [J]. Composites Science and Technology, 1988, 33(4): 257−277.

[13] GARGANO A, DONOUGH M, DAS R, et al. Damage to fibre-polymer laminates caused by surface contact explosive charges [J]. Composites Part B: Engineering, 2020, 197: 108162.

[14] ZHOU T Y. Research on dynamic response and failure mechanism of PVC foam sandwich structures under nearfield and contact blast loadings [D]. Wuhan: Huazhong University of Science and Technology, 2019 (in Chinese).

空爆载荷下碳纤维梯形波纹夹芯结构响应分析

章帅帅, 刘均*, 张攀, 程远胜

华中科技大学 船舶与海洋工程学院,湖北 武汉 430074

摘　要:[**目的**]研究迎爆面和背爆面面板厚度、壁板折角以及芯层高度对碳纤维增强复合材料梯形波纹夹层结构抗爆性能的影响规律。[**方法**]首先,基于三维Hashin失效准则,利用软件ABAQUS中的VUMAT用户子程序接口,开发纤维增强复合材料损伤演化的子程序模块;然后,通过与公开文献中的实验进行对比,验证爆炸冲击载荷下基于所开发子程序的碳纤维增强复合材料动态响应仿真方法的有效性;最后,基于该数值方法开展碳纤维增强复合材料梯形波纹板的抗爆性能参数化研究。[**结果**]结果显示,相比增大迎爆面面板的厚度,增大背爆面面板厚度对夹层板抗爆性能的提升更为明显;芯层壁板折角从45°减小至30°时,其抗爆能力提高了1.3%,而当从60°减小至45°时,其抗爆能力提高了6.3%;芯层高度从8 mm增大至20 mm时,其抗爆能力提高了27.7%。[**结论**]所做研究可为碳纤维增强复合材料夹层结构的抗爆设计提供参考。

关键词:复合材料;爆炸冲击;梯形波纹板;损伤演化;ABAQUS